

Predicting the Parasitic Forces in the Magnetically Levitated Adaptive Optics Mirrors

C. Del Vecchio^{*1}, R. Briguglio¹, M. Xompero¹, A. Riccardi¹

¹INAF-OAA

^{*}L. Enrico Fermi 5 I-50125 Firenze, Italy, cdelvecchio@arcetri.astro.it

Abstract:

In a voice-coil actuated deformable mirror, the controlling force is generated by the interaction between a magnet, bonded on the glass, and a current circulating in a wire, inserted in a reference frame. The misalignments between such two components, as well as the mutual interaction amongst the magnets, produce parasitic forces and torques. The evaluation of such effects is of crucial importance to model undesired deformations on the mirror optical surface. This paper discusses the Comsol models and the procedures implemented in order to compute these forces and torques: the proposed numerical methods are an alternative to complex, expensive, and time-consuming experimental tests.

Keywords: Adaptive Optics, Magnetostatics, Virtual Work

1 Introduction

The atmospheric turbulence affecting the telescope optics is corrected by the Adaptive Optics (AO) system by means of deformable optical surfaces. At the Large Binocular Telescope (LBT) and the Very Large Telescope (VLT) the deformations are actuated by voice-coil actuators, which provide a magnetic force generated by the interaction between a coil embedded in the Reference Frame (RF) and a permanent magnet, the *main magnet*, glued to the non-active surface of the deformable mirror (DM) — mechanically decoupled with respect to the RF (see Riccardi et al. [2008] and Gallieni and Biasi [2013]). If any mechanical misalignments between the DM and the RF occurs, the coaxiality of the main magnet with respect to both the coil and an auxiliary magnet, the *bias magnet* — responsible for the

restraining of the DM in case of electric failures and when the system is off — isn't fulfilled. Moreover, the DM isn't flat, so that it undergoes forces and torques due to the mutual magnetic interactions between the main magnets. Computing these two types of disturbances for any kind of voice-coil driven DM is the aim of this paper. The models discussed in the article are developed from the geometry and the materials of the LBT DM. On the back of its concave surface are glued 672, 1.8 mm thick compounds, with a center-to-center separation of ≈ 30 mm, built of Vacodym 510Hr — a very high energy density NdFe permanent magnet —, each arranged with eight 45° sectors, whose outer and inner diameters are 11 mm and 6 mm, respectively, and one central cylinder whose outer and inner diameters are 6 mm and 1 mm, respectively. While the latter is axially magnetized, the magnetizations of the eight sectors are perpendicular to the cylinder axis, oriented towards the center along the bisector. At a gap of of 400 μm , the RF hosts a 3 mm height coil with 270 turns, whose outer and inner diameters are 12 mm and 6 mm, and the cylindrical bias magnet, built of SmCo, whose outer diameter and height are, respectively, 1.9 mm and 4 mm, and whose bottom is separated by 2 mm from the main magnet top.

Each of the three available methods of computation of the magnetic forces — the Lorentz equation, the integration of the Maxwell stress tensor, and the principle of virtual work — must give two sets of forces and torques whose vector sum must be 0, according to the third principle of dynamics. The take the error of such a sum as the measure of the accuracy of the three methods. Because of its simplicity and accuracy, the first method is adopted for the coil-magnet interaction, as discussed in Sec. 4. The

magnet-to-magnet interactions, described in Sec. 5, requires the application of either the integration of the Maxwell stress tensor or the principle of virtual work. Although the former is available in Comsol without any additional computation, it doesn't give enough accuracy, in particular for the main magnet. Moreover, the Maxwell stress tensor should be computed on a surface very closely embedding the magnet, in order to increase the accuracy, with a consequent growing of the mesh complexity — and consequently of the number of degrees of freedom. For these reasons, the virtual work method is chosen. However, as an energy-based method, the virtual work computation requires a proper definition of both the stored energy and coenergy in the hard magnetic materials. In the most general case, so including non-linear permanent magnets, such energies can be defined as either via a Matlab[®] numerical integration or deploying the built-in Comsol integration operator — hence, the default Comsol definition of the magnetic energy is re-formulated, according to Sec. 1.

In order to reduce the number of degrees of freedom of the deformed geometry required to compute the forces via the virtual work method, in all the models the magnet domains are enclosed in a very thin (1 mm) air film — which, along with the magnet domains, are the only “Free Deformation” domains of the model. Finally, in order to avoid electromagnetic field singularities, the models are generated with fillets at the magnet/air interfaces. As a consequence, the mesh is properly refined in such areas, as depicted in Fig. 1. The various models sport from ≈ 3 from ≈ 10 millions of degrees of freedom.

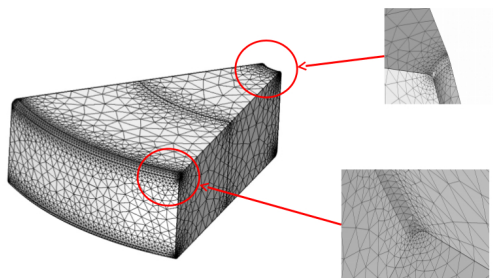


Figure 1: Detail of the mesh at a filleted corner.

Because of the complexity of the physics

and the geometry of the system and the rotations to be applied in order to properly compute the variation of the magnetic energy must be done around the principal axes of inertia — which, in the most general case, are not coincident with the XYZ Comsol geometry — the entire magnetic input is re-defined according to Sec. 3.

2 PM energies

In the most general case, the stored magnetic energy densities E and coenergy C are defined according to Eq. 1

$$E = \int_{B_0}^B H dB \quad C = \int_{H_0}^H B dH \quad (1)$$

According to Deliège et al. [2003], in the second quadrant of the B-H plane the magnetic energy and coenergy densities in a permanent magnet with retentivity B_r and coercivity H_c are defined according to Eq. 2

$$E = \int_{B_r}^0 H dB \quad C = \int_{H_c}^H B dH \quad (2)$$

Outside the second quadrant, that is when $B > B_r$ or $B < 0$ (and, consequently, when $H < H_c$ or $H > 0$), the permanent magnet behaves according to Eq. 1. Thus, E and C are to be rewritten as

$$E = \int_0^B H dB \times (B < 0) + \int_B^0 H dB \times (B \leq B_r) \times (B \geq 0) + \left(\int_{B_r}^0 H dB + \int_{B_r}^B H dB \right) \times (B > B_r) \quad (3)$$

$$C = \int_{H_c}^H B dH \times (H < H_c) + \int_{H_c}^H B dH \times (H \leq 0) \times (H \geq H_c) + \left(\int_{H_c}^0 B dH + \int_0^H B dH \right) \times (H > 0) \quad (4)$$

where the limits of the integrals are chosen in order to obtain positive values of E and C .

Because of the consecutiveness of the limits of the three integrals of Eq. 4, such an equation can be simplified as

$$C = \int_{H_c}^H B dH \quad (5)$$

A different definition of the magnetic energy density is proposed by Strahan [1998], Lovatt and Walterson [1999], and Campbell [2000]. According to them, in a permanent magnet E is defined as $\int_{B_r}^B H dB$, so that, for the same reasons which led to Eq. 3 and Eq. 4, the energy density is

$$E = \left(\int_{B_r}^0 H dB + \int_0^B H dB \right) \times (B < 0) + \int_{B_r}^B H dB \times (B \leq B_r) \times (B \geq 0) + \int_{B_r}^B H dB \times (B > B_r) \quad (6)$$

Because of the consecutiveness of the limits of the three integrals of Eq. 6, such an equation can be simplified as

$$E = \int_{B_r}^B H dB \quad (7)$$

A graphical visualization of the above defined energy and coenergy is reported on top of Fig. 2, which shows on bottom right, for a BH curve is plotted on bottom left, the difference between the energies defined in Equations 3, 5 and 6. As differentiating Equations 3 and 5 give the same force and torques results, while differentiating 7 gives a (moderately) lower accuracy, Eq. 5 — which is slightly less time consuming than Eq. 3 — is selected for the virtual work computations discussed in Sec. 5.

In order to properly compute the magnetic energy and coenergy densities, as in the most general case the computation can give $B > B_r$ and/or $B < 0$, the BH curve of the chosen material should be defined also in the first quadrant, as reported by instance by Volodchenkov et al. [2017].

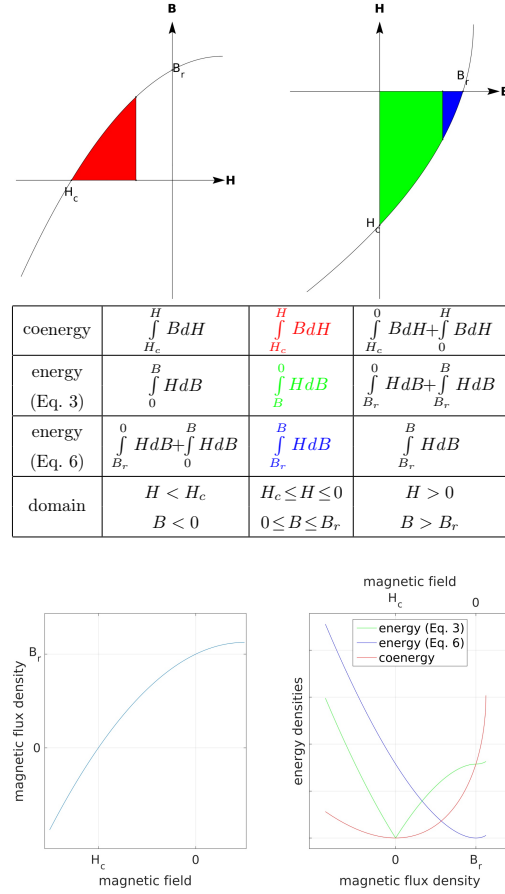


Figure 2: Meaning of E and C in the permanent magnet for $H_c \leq H \leq 0$ and $0 \leq B \leq B_r$ (top); integral limits needed to define the Equations 4, 3, and 6 (middle); comparison of Equations 3 and 6 (bottom).

3 Virtualization

We consider two coordinate systems and name the magnetic flux density as \mathbf{b} and \mathbf{B} , the magnetic field as \mathbf{h} and \mathbf{H} and the relative permeability as μ_r and \mathbf{M}_r in the two coordinate systems, respectively. The constitutive relations

$$\mathbf{b} = \mathbf{b}_r + \mu_0 \mu_r \mathbf{h} \quad (8)$$

and

$$\mathbf{B} = \mathbf{B}_r + \mu_0 \mathbf{M}_r \mathbf{H} \quad (9)$$

where \mathbf{b}_r and \mathbf{B}_r are the retentivities in the two coordinate systems, refer to the first and second coordinate systems, respectively. If \mathbf{T} is the transformation matrix that converts the first into the second coordinate system,

so that $\mathbf{B} = \mathbf{T}\mathbf{b}$, $\mathbf{B}_r = \mathbf{T}\mathbf{b}_r$, and $\mathbf{H} = \mathbf{T}\mathbf{h}$, Eq. 9 can be rewritten as

$$\mathbf{T}\mathbf{b} = \mathbf{T}\mathbf{b}_r + \mu_0\mathbf{M}_r\mathbf{T}\mathbf{h} \quad (10)$$

Premultiplying both terms of Eq. 10 by \mathbf{T}^{-1} , the transpose of \mathbf{T} , since $\mathbf{T}^{-1}\mathbf{T} = \mathbf{I}$, Eq. 10 becomes

$$\mathbf{b} = \mathbf{b}_r + \mu_0\mathbf{T}^{-1}\mathbf{M}_r\mathbf{T}\mathbf{h} \quad (11)$$

Comparing Equations 8 and 11 gives

$$\boldsymbol{\mu}_r = \mathbf{T}^{-1}\mathbf{M}_r\mathbf{T} \quad (12)$$

and, consequently

$$\mathbf{M}_r = \mathbf{T}\boldsymbol{\mu}_r\mathbf{T}^{-1} \quad (13)$$

Equations 8, 9, 12, and 13 can be easily implemented in Comsol to define the physics of the system avoiding the definition of any auxiliary coordinate system in Comsol when any kind of rotation (and displacement) have to be performed — including the (infinitesimal) ones implied by the virtual works. In particular, $\mathbf{B}_r = \mathbf{T}\mathbf{b}_r$ and Eq. 13 are used to define the constitutive relationship of the (typically anisotropic) permanent magnets as a function of any displacement and rotation. Although the NdBFe and the SmCo materials used in our models exhibit a very nearly linear BH curve, some test models show that implementing a non-linear permeability as a function of $|\mathbf{B}|$ or $|\mathbf{H}|$ by means of the Comsol interpolation tables gives accurate results.

Moreover, the rotations to be applied in order to properly compute the variation of the magnetic energy with the virtual works method must be done around the principal axes of inertia of a body. Defining the rotation vector $\boldsymbol{\theta} = [\theta_x; \theta_y; \theta_z]$, the transformation matrix that rotates the coordinate system $\mathbf{g} = [x; y; z]$, centered in the origin $[0; 0; 0]$, into the global coordinate system $\mathbf{G} = [X; Y; Z]$ is $\mathbf{G} = \mathbf{T}\mathbf{g} + \mathbf{C}$, and, consequently, $\mathbf{g} = \mathbf{T}^{-1}(\boldsymbol{\theta})(\mathbf{G} - \mathbf{C})$. where \mathbf{C} is the center of rotation of \mathbf{G} and $\mathbf{T} = \mathbf{Z} \times \mathbf{Y} \times \mathbf{X}$, being \mathbf{X} , \mathbf{Y} , and \mathbf{Z} defined according to Equations 14, 15, and 16, respectively.

$$\mathbf{X} = \begin{bmatrix} 1 & 0 & 0 \\ 0 & \cos\theta_x & -\sin\theta_x \\ 0 & \sin\theta_x & \cos\theta_x \end{bmatrix} \quad (14)$$

$$\mathbf{Y} = \begin{bmatrix} \cos\theta_y & 0 & \sin\theta_y \\ 0 & 1 & 0 \\ -\sin\theta_y & 0 & \cos\theta_y \end{bmatrix} \quad (15)$$

$$\mathbf{Z} = \begin{bmatrix} \cos\theta_z & -\sin\theta_z & 0 \\ \sin\theta_z & \cos\theta_z & 0 \\ 0 & 0 & 1 \end{bmatrix} \quad (16)$$

If we define the rotation vector $\boldsymbol{\beta} = [\beta_x; \beta_y; \beta_z]$, where β_x , β_y , and β_z are the rotation along the local axes x , y , and z , respectively, the local displacement is $\boldsymbol{\delta} = \mathbf{D}\mathbf{g} - \mathbf{g}$, where \mathbf{D} is defined as \mathbf{T} , substituting δ_x , δ_y , and δ_z with β_x , β_y , and β_z , respectively. Thus, the global displacement is $\boldsymbol{\Delta} = \mathbf{T}\boldsymbol{\delta} = \mathbf{T}\mathbf{D}\mathbf{g} - \mathbf{T}\mathbf{g}$. As a consequence, the final coordinate system $\mathbf{G}' = [X'Y'Z']$, defined as $\mathbf{G}' = \mathbf{G} + \boldsymbol{\Delta}$, is equal to $\mathbf{T}\mathbf{g} + \mathbf{C} + \mathbf{T}\mathbf{D}\mathbf{g} - \mathbf{T}\mathbf{g}$, that is

$$\mathbf{G}' = \mathbf{T}\mathbf{D}\mathbf{g} \quad (17)$$

The transformation matrix \mathbf{F} that transform the local coordinate system \mathbf{g} into \mathbf{G}' is

$$\mathbf{F} = \mathbf{T}\mathbf{D} \quad (18)$$

Choosing x , y , and z as the principal axes of inertia of the magnet of which we have to compute the force, we use Eq. 18 throughout all the models in order to define the virtual displacements caused by the rotations $\boldsymbol{\beta}$ without defining any auxiliary coordinate system, thus reducing the computational complexity.

4 Magnet-coil

The forces f and the torques t due to a displacement δ and a rotation θ of the magnet with respect to the coil are computed with the Lorentz equation and are summarized in Figures 3 and 4, where f and t are plotted versus δ_x and θ_x of the main magnet — f and t versus δ_y and θ_y of the coil and/or the main magnets being very close due to the main magnet magnetizations. Both the *parasitic* effects (f_x and t_y for δ_x , f_y and t_x for δ_y ; f_y and t_x for θ_x , f_x and t_y for θ_y) are very close to linearity. The *active* f_z is practically a constant, and the *parasitic* f_x and f_y are always below the 3% of f_z , even for alignments tolerances as large as ± 1.1 mm or $\pm 1.5^\circ$.

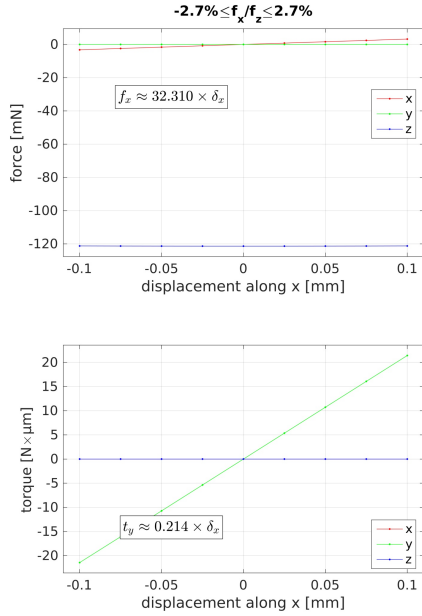


Figure 3: f and t for main magnet δ_x .

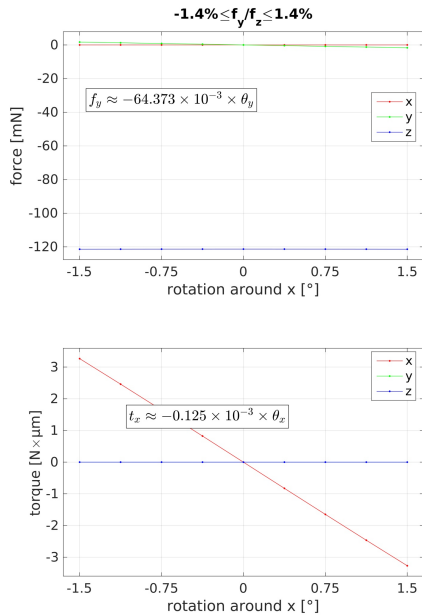


Figure 4: f and t for main magnet θ_x .

5 Magnet-magnet

5.1 Crosstalk

In principle, each magnet glued on the back (non active) surface of the DM is magnetically coupled with all the other magnets. This force decays very rapidly with the distance. Because the magnets are all spaced by ≈ 30 mm, only two interactions are considered: the magnetic force between the actuators 1 and 2, located on the first ring of

actuators at radius 43.044 mm and separated by angle β equal to 44° , and the magnetic force between the actuators 1 and 10, located on the x axis and separated by a distance δ equal to 30.31 mm. In both cases the virtual works computation poorly verifies the third principle of dynamics, so that we run two sets of computations: instead of computing the interaction between two actual pairs of magnets, in the first case, the angular separation is increased from $\beta = 18^\circ$ by steps of 1° , in the second one the distance is increased from $\delta = 14$ mm by steps of 1 mm. In both runs, the analysis is halted if the angle between the two forces and torques is $< 170^\circ$ or if the difference between the norms of the forces and the torques is $> 2\%$. Fitting the computed forces and torques as a function of β and δ , respectively, with the *Two-Term Exponential Model* of the *curvefit* toolbox of Matlab[®] shown in Eq. 19, allows to define the above mentioned interactions — namely the force F and the torques T_1 and T_2 with respect to the mean plane of the DM at the nominal locations of the two magnets, respectively — by means of the parameters listed in Tab. 1, with fitting errors $\leq .25\%$ for $14 \text{ mm} \leq \delta \leq 18 \text{ mm}$ and $\leq .6\%$ for $18^\circ \leq \delta \leq 25^\circ$. The directions of F and T_1 and T_2 are shown in Fig. 5 for $\beta = 18^\circ$ and for $\delta = 14$ mm. Eq. 19 gives $F = 0.657 \text{ mN}$, $T_1 = 4.070 \text{ N} \times \mu\text{m}$, and $T_2 = 4.143 \text{ N} \times \mu\text{m}$, for $\beta = 40^\circ$, and $F = 0.959 \text{ mN}$, $T_1 = 6.617 \text{ N} \times \mu\text{m}$, and $T_2 = 5.656 \text{ N} \times \mu\text{m}$, for $\delta = 28$ mm. As such values are very low — the typical turbulence-correction force is $\approx .4 \text{ N}$ rms and the maximum dynamic force is $\approx 1.3 \text{ N}$ — the strengths on the mirror shell are totally negligible — also, as the sums of these forces and torques are null, they don't affect the DM global statics. Nevertheless, Eq. 19 and Tab. 1. allow to determine a lower limit for the actuator separation.

$$f(x) = C_1 e^{k_1 x} + C_2 e^{k_2 x} \quad (19)$$

$f(x)$	x	C_1	k_1	C_2	k_2
F		16550.3	-37.4582	5.09809	-12.8304
T_1	β	18.9089	-35.088	0.0097198	-11.1418
T_2		12.7918	-33.9237	0.00780015	-10.8013
F		21777.2	-900.256	6.56426	-313.77
T_1	δ	10.64	-775.193	0.00771193	-250.873
T_2		21.5468	-836.01	0.0112864	-269.964

Table 1: The parameters used to fit the exponential decay (see Eq. 19).

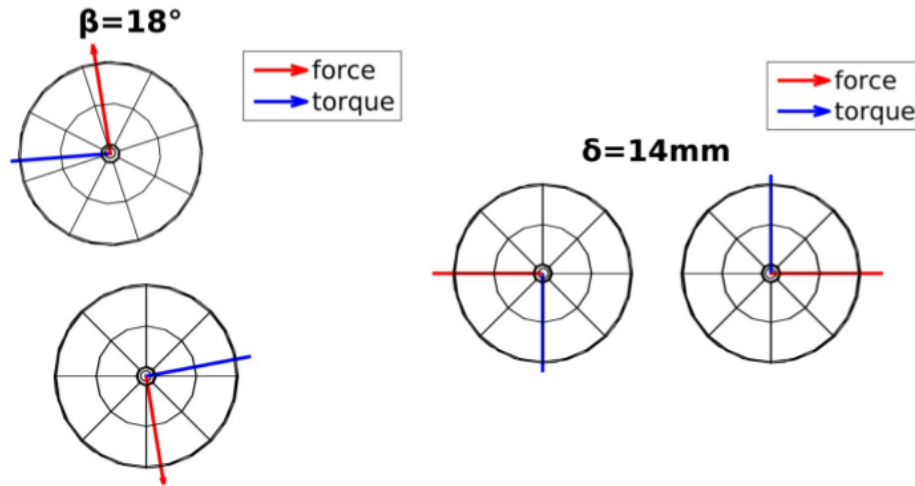


Figure 5: Top view of the two main magnets separated by $\beta = 18^\circ$ (left) and by $\delta = 14\text{ mm}$ (right).

5.2 Bias

The forces and the torques due to a displacement and a rotation of the main magnet with respect to the bias magnet, computed with the virtual works method, are summarized in Fig. 6, where the forces f_x , f_y , and f_z and the torques t_x , t_y , and t_z are plotted versus the x displacements and rotations of

the main magnet — the forces and torques versus the y displacements/rotations of the bias magnet and/or the main magnets being very close due the geometry of the main magnet magnetizations. In both cases the force parallel to the displacement, is a small fraction ($\leq 2\%$ for $|\delta| \leq .1\text{ mm}$ and $|\theta| \leq 1^\circ$) of f_z , and the torques are $\leq 10\text{ N} \times \mu\text{m}$, totally tolerable.

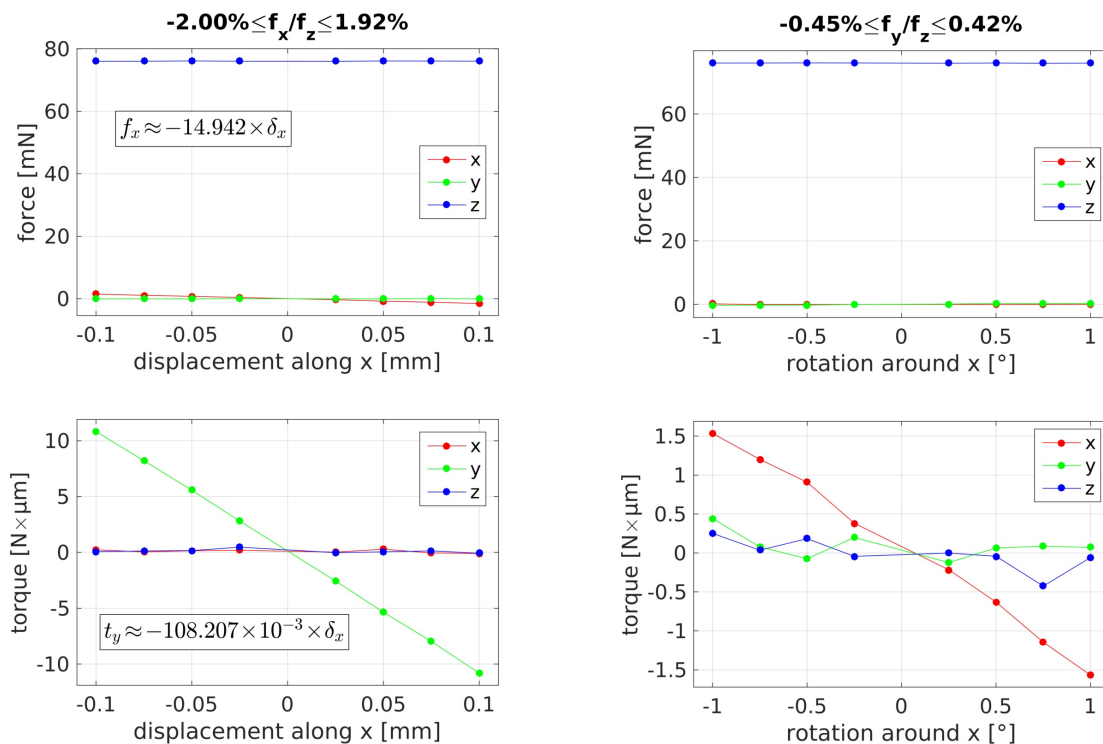


Figure 6: Forces and torques for main magnet x displacements (left) and x rotations (right).

6 Conclusions

We investigated the parasitic magnetic forces and torques affecting a deformable mirror controlled via voice-coil actuators. We addressed in particular two cases: the magnet-to-coil/bias versus their relative misalignments and the mutual magnet-to-neighbor magnet interaction. The analysis is carried out by the implementation of the virtual work principle in Comsol. We considered the particular case of the Large Binocular Telescope Deformable Mirror. The simulation results show tolerable values. In fact, the crosstalk between the permanent magnets gives forces three orders of magnitude lower than the typical correction force and torques of few $N \times \mu m$, while the interactions between main magnet and coil or bias magnet give parasitic effects within few percent of the active force and torques $< 100 N \times \mu m$ even in the worst, overestimated misalignment case. The proposed method is a valuable tool to predict the minimum actuator spacing for the future, possible high spatial-density, large deformable mirrors and to define the tolerances when manufacturing a component as delicate as an Adaptive Optics system.

References

- P. Campbell. Comments on "Energy stored in permanent magnets". *IEEE Transactions on Magnetics*, 36(1):401–403, jan 2000. doi: 10.1109/20.822554. URL <https://doi.org/10.1109/2F20.822554>.
- G. Delière, F. Henrotte, H. Vande Sande, and K. Hameyer. 3D h-phi finite element formulation for the computation of a linear transverse flux actuator. "COMPEL", 22(4):1077–1088, 2003. ISSN 0332-1649. doi: 10.1108/03321640310483011.
- D. Gallieni and R. Biasi. The new VLT-DSM M2 unit: construction and electromechanical testing. In S. Esposito and L. Fini, editors, *Third AO4ELT Conference*, Proc. AO4ELT. AO4ELT, 5 2013. doi: 10.12839/AO4ELT3.17883.
- H. Lovatt and P. Walterson. Energy stored in permanent magnets. *IEEE Transactions on Magnetics*, 35(1):505–507, 1999. doi: 10.1109/20.737473. URL <https://doi.org/10.1109/2F20.737473>.
- A. Riccardi, M. Kompero, D. Zanotti, L. Busoni, C. Del Vecchio, P. Salinari, P. Ranfagni, G. Brusa Zappellini, R. Biasi, M. Andrighettoni, D. Gallieni, E. Ancalerio, H. M. Martin, and S. M. Miller. Adaptive secondary mirror for the Large Binocular Telescope: results of acceptance laboratory test. In C. E. Max, P. L. Wizinowich, and N. Hubin, editors, *Adaptive Optics Systems*, volume 7015 of *Proc. SPIE*, pages 12.1–12.9. SPIE, 6 2008.
- R. Strahan. Energy conversion by nonlinear permanent magnet machines. *IEE Proceedings - Electric Power Applications*, 145(3):193–198, 1998. doi: 10.1049/ip-epa:19981863. URL <https://doi.org/10.1049/2Fip-epa%3A19981863>.
- A. Volodchenkov, S. Ramirez, R. Samnakay, R. Salgado, Y. Kodera, A. Balandin, and J. Garay. Magnetic and thermal transport properties of SrFe₁₂O₁₉ permanent magnets with anisotropic grain structure. *Materials & Design*, 125:62 – 68, 2017. ISSN 0264-1275. doi: <https://doi.org/10.1016/j.matdes.2017.03.082>. URL <http://www.sciencedirect.com/science/article/pii/S0264127517303374>.